Analysis of Damage of Asphalt Pavement due to Dynamic Load of Heavy Vehicles Caused by Surface Roughness

T. Kanai, K. Tomisawa and T. Endoh
Technical Research Institute, Kajima road Co., Ltd., Chofu, Tokyo, Japan

K. Himeno
Department of Civil and Environmental Engineering, Chuo University, Bunkyo, Tokyo, Japan

ABSTRACT: Roughness of asphalt pavement affects the ride quality and also generates dynamic load of heavy vehicles to give the pavement structure additional damage. However, few studies about the deviation of dynamic load and its influence to the structural damage of the pavement have been performed. So, we have conducted the following computer simulation. 1) *IRI* is settled at eight levels from 0.5 to 4.0 at 0.5 intervals, 2) pavement profiles are calculated for each level of *IRI* by the computer program that we have developed by adopting the random motion of Brownian oscillator at the end of a spring, 3) the running simulation is performed at various running speed using the packaged software, TruckSim into which the pavement profiles are inputted, 4) tensile strain at the bottom of the asphalt layer and compressive strain at the top of the subgrade is calculated by multi-layered elastic computer program on base of the dynamic load simulated above, and the damage of pavement is also analyzed. From these results, it is found that both of the dynamic load and the strain as pavement response tends to change more significantly according to increase of *IRI* or running speed. Large variation of strain generates the point where the permissive repetition loading time is very small, or the pavement life is very short. The result of analysis throughout the study section also reveals that the pavement damage increases due to increase of *IRI*, and its increasing degree becomes more remarkable as running speed is high.

KEY WORDS: Profile, *IRI*, asphalt pavement, dynamic load, fatigue damage.

1 INTRODUCTION

The roughness of road surface greatly affects the comfort of vehicle occupants. It has also been pointed out that surface roughness induces dynamic vehicle loads during the running of the vehicle and serves as a cause of promotion of damage to the pavement (Cebon 1999).

In order to verify the effects of surface roughness on the damage to asphalt pavement, eight levels of international roughness indexes (*IRI*s) were established and road surface profiles were prepared for respective *IRI*s. Measuring profile data on actual roads was expected to require a considerable amount of time and effort. Then, a method was developed to generate road profiles following the trace of the Brownian movement of a spring oscillator considering the randomness of surface roughness.

The generated profiles were incorporated into running simulation packaged software to simulate running using a vehicle model while varying the running speed. The dynamic wheel

loads at respective speeds obtained by simulation were given to an asphalt pavement model considering the effects of the loading time for conducting multi-layer elasticity analysis. Strains at the bottom of the asphalt layer and at the top of the subgrade in response to loading were obtained by conducting the above analysis, and substituted in Japan's fatigue failure standard equations to calculate the allowable number of repetitions of wheel passage and the damage to the pavement.

As a result, a possibility of local breakdown or great damage throughout the study section with the increase of *IRI* or running speed could be quantitatively identified.

2 METHODS FOR GENERATING ROAD PROFILES, SIMULATING VEHICLE RUNNING AND ANALYZING DAMAGE TO THE PAVEMENT

This study is conducted in three steps: generating road profiles, simulating vehicle running and analyzing the damage to the pavement in Figure 1. The methods in respective steps are described in detail below.

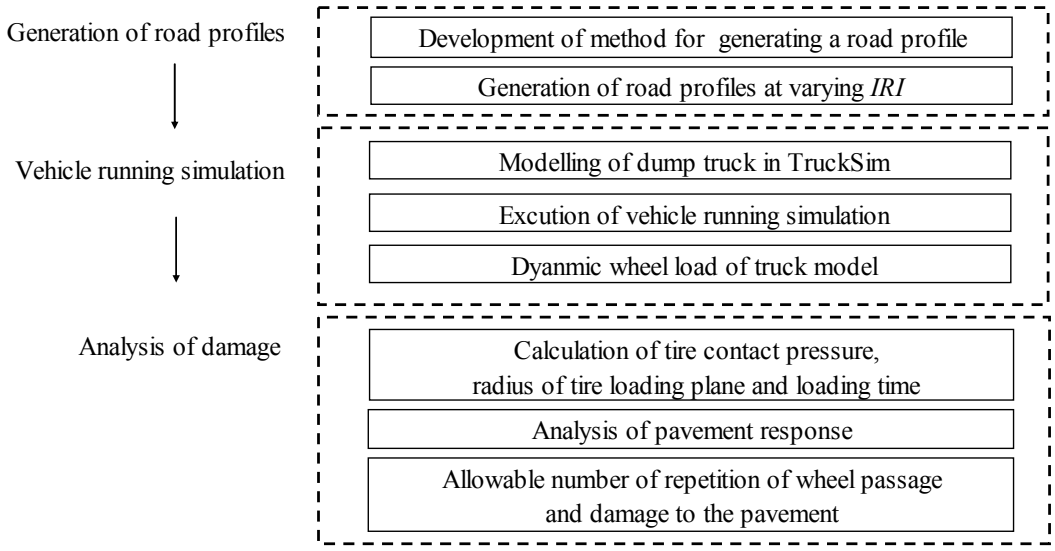

Figure1: Methodology in this study.

2.1 Method for Generating Road Profiles

If the surface profile is known, surface roughness can be evaluated and the comfort of vehicle occupants and damage to the pavement can be analyzed using *IRI*s. Measuring surface profile data accurately, however, requires costly equipment and much time and effort. Then, the authors developed a method for representing random surface roughness by the trace of the Brownian movement of a spring oscillator and generating a road profile at a given *IRI* on a personal computer screen. Road profiles were generated for the designated eight *IRI* levels using the method.

2.1.1 Trace of the Brownian Movement of a Spring Oscillator

The motions of the oscillator at the tip of a spring are simple harmonic in accordance with Newton's law. Subjected to the actions of cohesive resistance or collision, the motions are Brownian movements. The movement is expressed using Equation (1) by incorporating the elements of Langevin equation (Yonezawa 1986).

$$m\frac{d^2x}{dt^2} = -Kx - \zeta\frac{dx}{dt} + F(t) \quad (1)$$

where, x is the displacement of the oscillator, t is time, m is the mass of the oscillator, K is spring constant, ζ is cohesive resistance and $F(t)$ is applied force.

On the right side of Equation (1), the first, second and third terms indicate the force acting from the spring on the oscillator, damping of speed due to cohesive resistance and fluctuation due to the collision force acting on the oscillator, respectively. The randomness of collision force $F(t)$ is governed by the random number that represents the fluctuation and by temperature that determines thermal motion. For solving kinematic Equation (1), numerical analysis was conducted by the Runge-Kutta method, and an approximate solution was obtained for the displacement of the oscillator.

2.1.2 Effects of Temperature and Cohesive Resistance on *IRI*

The displacement of the oscillator was calculated based on the assumption of a fixed mass of the oscillator and a fixed spring constant at three varying levels of temperature and cohesive resistance shown in Table 1.

Table 1: Variables for calculation.

Vaiables	Values
Temperature	750, 1500, 3000
Cohesive resistance	1, 5, 10

Calculations were made in 1100 steps at intervals of 0.01 seconds. Displacements were extracted from 101st step to 1100th step where a stable state was reached. Regardless of the physical implications of calculation conditions and results, a 250-m-long surface profile was generated by using the displacements extracted as road surface elevations at intervals of 250 mm. The process was repeated three times under each calculation condition. For the road profile obtained, *IRI* was calculated by ProVAL2.73 program available on the Internet. The calculation results are shown in Table 2.

Table 2: Calculation result of *IRI*.

Variables		*IRI*					
Temperature	Cohesive resistance	1st	2nd	3rd	Average	Standard devision	Coefficient of variation
750	1	1.15	1.36	1.12	1.21	0.13	10.8
750	5	0.77	0.67	0.75	0.73	0.05	7.2
750	10	0.54	0.58	0.54	0.55	0.02	4.2
1500	1	2.05	2.19	2.28	2.17	0.12	5.3
1500	5	1.40	1.59	1.75	1.58	0.18	11.1
1500	10	0.91	1.06	1.15	1.04	0.12	11.7
3000	1	5.13	5.86	3.99	4.99	0.94	18.9
3000	5	2.70	2.93	2.88	2.84	0.12	4.3
3000	10	2.08	2.29	2.38	2.25	0.15	6.8

Table 2 shows that the greater the cohesive resistance, the lower the *IRI* as long as the temperature was fixed. While the cohesive resistance was fixed, the higher the temperature, the higher the *IRI*. Both temperature and cohesive resistance were found to have a correlation with *IRI*. Multiple regression analysis was therefore made using temperature and cohesive

resistance as explanatory variables. For *IRI*, an objective variable, a logarithm was adopted in view of its nonlinear relationship with an explanatory variable. The regression equation obtained by analysis is shown in Equation (2). Equation (2) has a high coefficient of determination and is highly accurate. Specifying temperature and cohesive resistance so as to satisfy the equation and obtaining the variation of the spring oscillator enable the generation of a road profile at a designated *IRI*.

$$\log(IRI) = 0.00026T - 0.03668\zeta - 0.06699 \quad (r^2=0.95) \tag{2}$$

where, T is temperature and ζ is cohesive resistance.

2.1.3 Generation of Road Profile in This Study

In this study, eight *IRI* levels were established from 0.5 to 4.0 m/km at a pitch of 0.5 m/km, and the combination of temperature and cohesive resistance was properly specified using Equation (2) to generate road profiles for respective *IRI* levels.

2.2 Method of Vehicle Running Simulation

After the generation of road profiles, vehicle running simulation was made for a model of a dump truck generally used in Japan by TruckSim, a vehicle running simulation program, to obtain the dynamic wheel loads applied during the running of the vehicle at intervals of 0.01 second. A 20-ton dump truck was employed as the model (see Figure 2) running at four levels of speed, 40, 60, 80 and 100 km/h.

TruckSim is simulation software running on a personal computer that was developed as a result of research at the University of Michigan. The software enables quick and easy analysis and evaluation of the dynamic behavior of large vehicles such as trucks and buses under various operation conditions (e.g. operation of accelerator, brake pedal and steering wheel) and environmental conditions (e.g. surface friction coefficient and changes in surface elevation).

	Axle load (kN)	Wheel type	Wheel position
Steering axle	63.6	Single tire	
Front axle of tandem axle	66.2	Dual tire	
Rear axle of tandem axle	66.4	Dual tire	

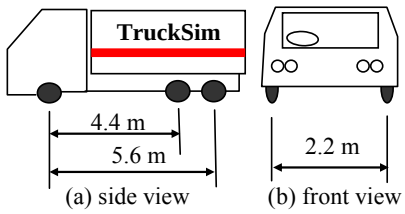

Figure2: Specification of truck model.

2.3 Method for Analyzing Damage to the Pavement

For analyzing the damage to the pavement, the contact pressure, radius of loading and loading time were obtained based on the running speed and dynamic wheel load, and the elastic modulus of the asphalt layer was calculated from the values representing the properties of specified asphalt and asphalt mixture. Finally, the response of the pavement was substituted in the failure standard equation to calculate the allowable number of repetitions of wheel passage and damage to the pavement defined as the reciprocal of the allowable number of repetitions of wheel passage.

2.3.1 Calculation of Tire Contact Pressure, Radius of Loading plane and Loading Time

Ikeda and Ito (Ikeda and Ito 1985) examined the relationship of tire pressure and wheel load to tire contact pressure while varying the first two parameters using various types of tires. As a result, they proposed two formulas for obtaining tire contact pressure in cases where grooves of tires are taken into consideration and otherwise. In this study, Equation (3), the more severe equation with no grooves, was adopted. An ordinary tire pressure of 0.59 MPa was used.

$$p = 0.00489P + 0.373A + 0.218 \tag{3}$$

where, P is wheel load (kN), A is tire pressure (MPa) and p is tire contact pressure (MPa).

Next, the radius of loading plane was obtained using Equation (4) on the assumption that the load contacts the ground via a circular plane.

$$r = \sqrt{1000P/(\pi \cdot p)} \tag{4}$$

where, r is the radius of loading plane (mm)

The loading time was defined as the time required to travel the distance equivalent to the diameter of the tire contact surface at a designated speed, and was calculated by Equation (5).

$$t = 2r/v \tag{5}$$

where, t is the loading time (s) and v is the speed (mm/s).

2.3.2 Analysis of Pavement Response

Asphalt and asphalt mixture of ordinary properties listed in Table 3 were assumed and temperature was set at 20 degree C, and their stiffness (elastic modulus) was obtained at each loading time specified above. For estimating the stiffness of the asphalt, the nomograph of Van der Poel (Van der Poel 1954) was used. For final calculation of the stiffness of the asphalt mixture, the Shell's equation proposed by Heukelom and Klomp (Heukelom and Klomp 1964) was used. At the time of interpretation of the nomograph and calculations using equations, on a personal computer, the SbitSmix program was used that was developed by the authors for automatic processing because large quantities of data were involved.

Table 3: Ordinary properties of asphalt and asphalt mixture.

	Terms	Value
Asphalt	Penetration (1/10mm)	54
	Softening point (℃)	52
Asphalt mixture	Asphalt volume (%)	13
	Void content (%)	4

Next, a four-layer model of the asphalt pavement was built (see Figure 3), dynamic wheel loads were applied as dual-tire circular uniformly distributed loads, and the tensile strain at the bottom of the asphalt layer and the compressive strain at the top of the subgrade were

calculated, which were critical when considering fatigue failure, using GAMES, a multi-layer elasticity analysis program (JSCE 2005). Center to center distance between tires, thickness of each layer, elastic modulus E and Poisson's ratio v were fixed as shown in Figure 3. The radius r of contact area and elastic modulus (stiffness) of the asphalt layer as described above were assumed to be variable according to the dynamic load.

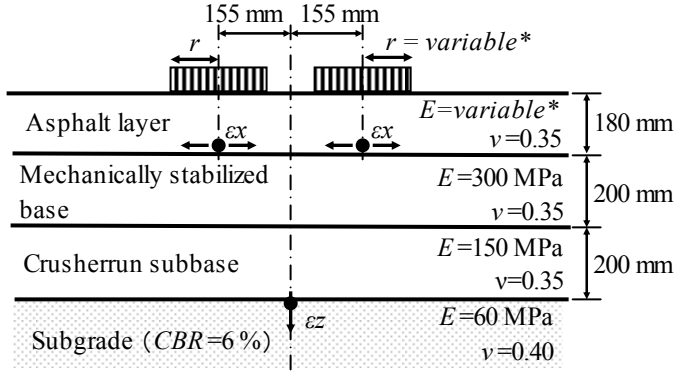

* For example
P = 16.6 kN (half of dual tire's load)
p = 0.52 MPa
r = 101 mm
speed = 100 km/h
t = 0.0073 s
E (asphalt layer) = 5700 MPa

Figure3: Pavement model with wheel load of dual tire for damage analysis.

2.3.3 Allowable Number of Repetitions of Wheel Passage and Damage to the Pavement

The responses of the pavement (tensile strain at the bottom of the asphalt layer and compressive strain at the top of the subgrade) were substituted in the fatigue failure standard equations concerning the cracking of asphalt layer and the rutting due to the deformation of subgrade (Equations (6) and (7), respectively) (Japan Road Association 2006) to obtain the allowable number of repetitions of wheel passage. Equation (6) is used to calculate the allowable number of repetitions of wheel passage up to a point where the cracking ratio reaches 20%. Equation (7) is used to calculate the allowable number of repetitions of wheel passage up to a point where the rut depth due to permanent deformation reaches 15 mm.

$$N_{fa} = \beta_{a1}(C) \cdot \left(6.167 \times 10^{-5} \cdot \varepsilon_x^{-3.291\beta_{a2}} \cdot E^{-0.854\beta_{a3}}\right) \quad (6)$$

where,
N_{fa}: Allowable number of repetitions of wheel passage
C: Parameter concerning the volume characteristics of a mixture used on the lowest level of the asphalt layer ($C = 10^M$ with $M = 4.84(VFA/100\text{-}0.69)$ and VFA: Degree of saturation)
ε_x: Tensile strain at the bottom of the asphalt layer (μ)
E: Elastic modulus (stiffness) of a mixture used in the lowest level of the asphalt layer (MPa)
β_{a1}, β_{a2} and β_{a3}: Correction factors for the failure standard equation of the Asphalt Institute specified based on the experience in Japan ($\beta_{a1} = 5.229 \times 10^4$, $\beta_{a2} = 1.314$, $\beta_{a3} = 3.018$)

$$N_{fz} = \beta_{s1}\left(1.365 \times 10^{-9} \cdot \varepsilon_z^{-4.477\beta_{s2}}\right) \quad (7)$$

where,
ε_z: Compressive strain at the top of the subgrade (μ)
β_{s1} and β_{s2}: Correction factors for the failure standard equation of the Asphalt Institute specified based on the experience in Japan ($\beta_{s1} = 2.134 \times 10^3$, $\beta_{s2} = 0.819$)

The damage to the pavement was defined as the reciprocal of the allowable number of repetitions of wheel passage. The damage throughout the study section was represented by the hatch-type area surrounded by the points of damage as shown in Figure 4.

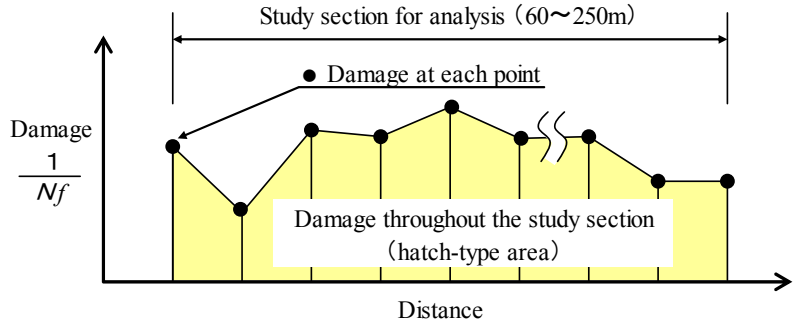

Figure 4: Schematic of damage throughout the study section.

3 RESULTS OF ANALYSIS

Shown below are the results of analysis of road profiles, dynamic wheel loads, allowable number of repetitions of wheel passage and damage to the pavement obtained using the method described above.

3.1 Generation of Road Profiles at Varying *IRI*s

The proposed method was used to generate 250-m-long road profiles at eight *IRI* levels from 0.5 to 4.0 m/km at pitches of 0.5 m/km. Typical profiles at *IRI* levels of 0.5, 1.5, 3.0 and 4.0 m/km are shown in Figure 5. The figure shows that the fluctuations of road profile increased with the *IRI* level.

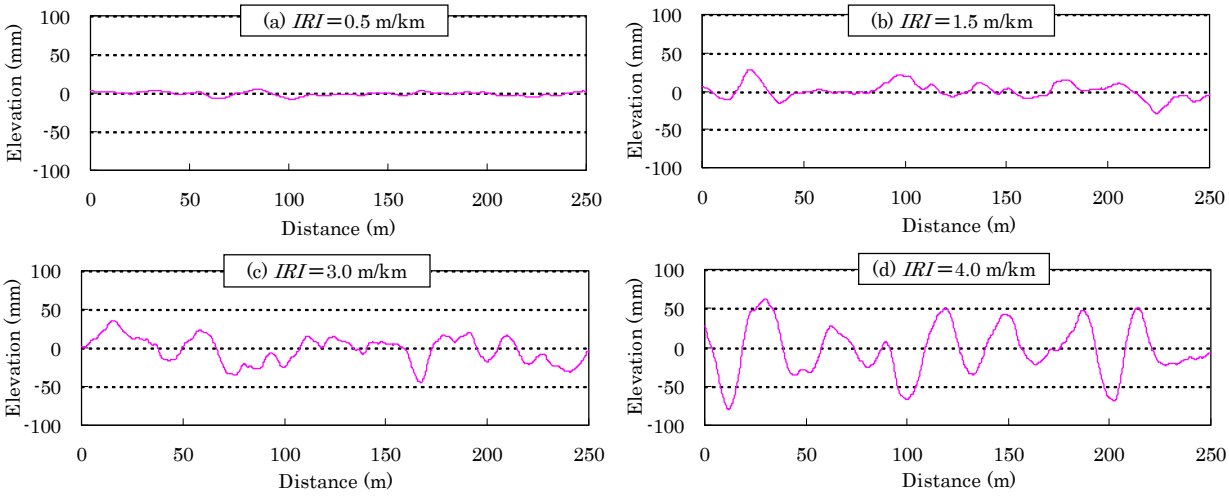

Figure 5: Typical 250-m-long road profiles generated at four *IRI* levels ((a) 0.5 m/km, (b) 1.5 m/km, (c) 3.0 m/km, (d) 4.0 m/km)

3.2 Dynamic Wheel Loads in Running Simulation

The road profiles generated were incorporated into TruckSim. Running simulation was made using a vehicle model shown in Figure 2 to obtain the dynamic loads of respective wheels.

Running speeds adopted were 40, 60, 80 and 100 km/h. Data collected in a section between points 60 through 250 m from the start of the test section after the vehicle model started stable running was adopted.

A result is shown in Figure 6 (*IRI*=40 m/km, running speed=100 km/h). The figure shows that wheel loads fluctuated more considerably for the tandem axles than for the steering axle. Only a slight difference was found in dynamic wheel load between the front and rear axles of tandem axle. The maximum dynamic wheel load occurred in the rear axle of tandem axle.

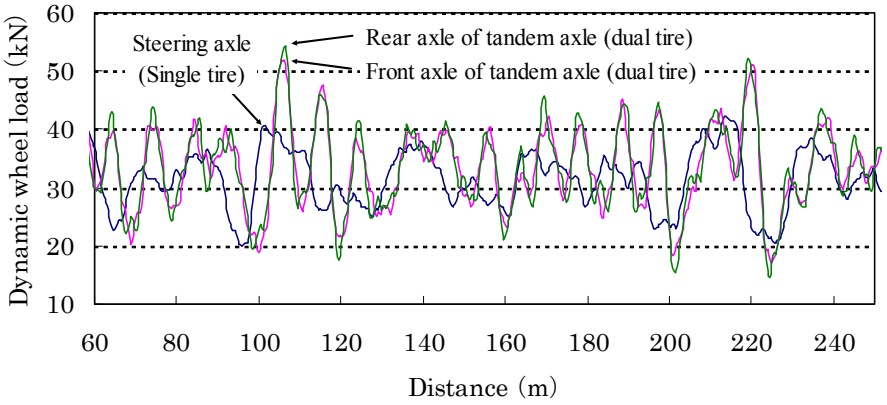

Figure 6: Example of dynamic wheel loads at *IRI*=4.0 m/km and speed=100 km/h.

Focus was placed on the rear axle of tandem axle where the maximum dynamic load occurred. The distribution of dynamic wheel loads was investigated at each *IRI* level at different speeds. The results are shown in Figure 7. Dynamic loads were nearly normally distributed under any condition. It was verified that the higher the *IRI* and the speed, the larger the amplitude of variation and the larger the maximum value of dynamic wheel load.

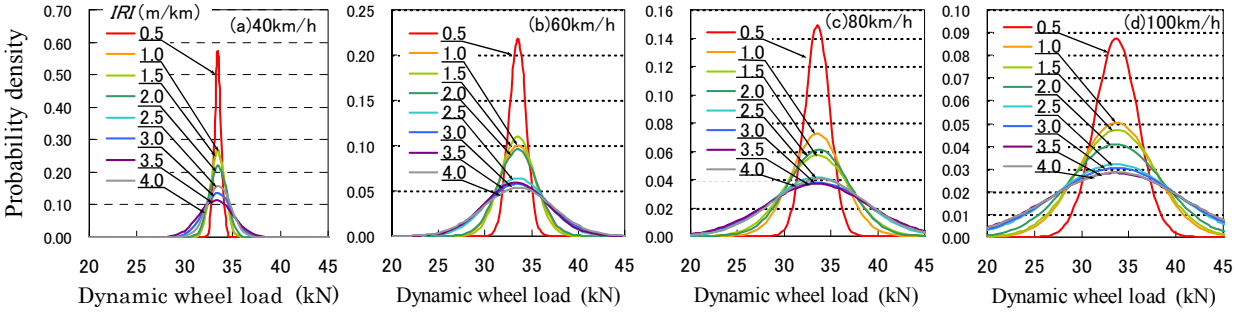

Figure 7: Distributions of dynamic wheel loads on rear axle of tandem axle at each *IRI* level at four speed levels ((a) 40 km/h, (b) 60 km/h, (c) 80 km/h, (d) 100 km/h).

3.3 Analysis of Damage to the Pavement

3.3.1 Pavement Response

The tensile strain ε_x at the bottom of the asphalt layer and the compressive strain ε_z at the top of the subgrade in a pavement model shown in Figure 3 were calculated by multi-layer elasticity analysis under the dynamic wheel load (rear axle of tandem axle, dual tire) obtained in running simulation using TruckSim. The typical strains calculated are shown in Figures 8 (a) and (b). A comparison of (a) and (b) shows that the variation of strains on the asphalt layer and subgrade increased considerably with the increase of *IRI* and speed.

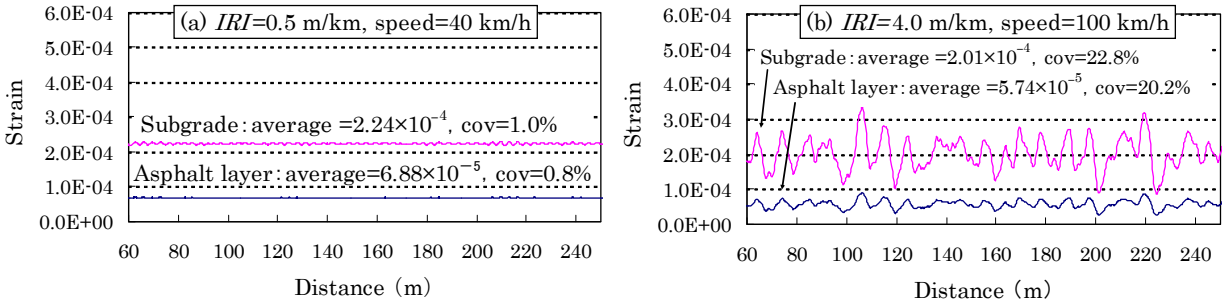

Figure 8: Calculation results of strain at the asphalt layer and the subgrade at two sets of *IRI* and speed ((a) 0.5 m/km, 40 km/h, (b) 4.0 m/km, 100 km/h).

3.3.2 Allowable Number of Repetitions of Wheel Passage

The tensile strain ε_x at the bottom of asphalt layer and the compressive strain ε_z at the top of the subgrade were substituted in Equations (6) and (7), respectively, which are temporary failure standard equations developed to meet the local conditions based on the failure standard equations of the Asphalt Institute, to calculate the allowable number of repetitions of wheel passage in respective layers. The typical allowable number of repetitions of wheel passage calculated are shown in Figures 9 (a) and (b).

Figures 9 (a) and (b) show that variation increased with *IRI* and speed. The coefficient of variation of allowable number of repetitions of wheel passage exceeded 100%. Considering the fact that the failure of pavement starts at a point with the lowest allowable number of repetitions of wheel passage, the results seem to suggest that pavements are likely to suffer local failure with the increase of *IRI* and speed.

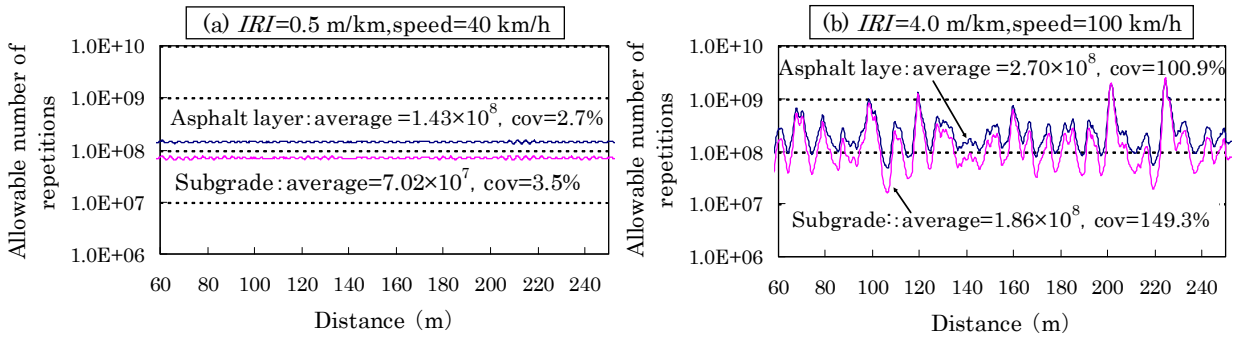

Figure 9: Calculation results of allowable number of repetitions of wheel passage at two sets of *IRI* and speed: ((a) 0.5 m/km, 40 km/h, (b) 4.0m/km, 100 km/h).

3.3.3 Damage to the Pavement by Dynamic Wheel Load

Based on the allowable number of repetitions of wheel passage calculated, damage to the asphalt layer and subgrade at each point due to a round of wheel loading (1/allowable number of repetitions of wheel passage) was calculated. Damage throughout the analysis section was obtained as shown in Figure 4. The damage throughout the section at each speed at *IRI* of 0.5 m/km was used as a basis (1.0) either for the asphalt layer and subgrade. Then, the ratio to the damage at each *IRI* level was obtained. The results are shown in Figures 10 (a) and (b). The damage throughout the section increased with the increase of *IRI* either for the asphalt layer and subgrade, and the tendency was more outstanding at higher speeds. The damage was expected to increase by 10 to 20% at the maximum at a running speed of 100 km/h.

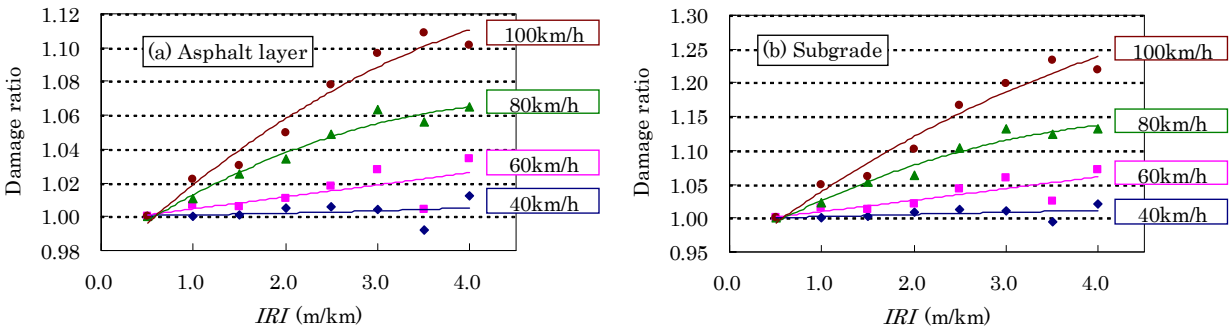

Figure 10: Relationship between *IRI* and Damage ratio ((a) asphalt layer, (b) subgrade).

4 SUMMARY

The results of this study are summarized below:

(1) A method was developed to generate road profiles based on the trace of the Brownian movement of a spring oscillator.

(2) Road profiles were generated at eight *IRI* levels on a personal computer using the developed method. Running simulation was made using TruckSim at four running speeds to obtain dynamic wheel loads.

(3) It has been verified that dynamic wheel loads fluctuate greatly with the increase of *IRI* and running speed, and that the response strain of pavement also exhibits similar tendency.

(4) It has finally been found that extremely low allowable number of repetitions of wheel passage occurs at some points either for asphalt layer or subgrade, and that local damage to pavement is highly likely to occur.

(5) It has been quantitatively verified that the damage throughout a section either for asphalt layer or subgrade increases as *IRI* (roughness) increases, and that the rate of increase is higher at higher running speeds.

This study confirmed that the service life of pavement (allowable number of repetitions of wheel passage) is affected by *IRI* that is an indicator of roughness and running speed. In the future, surface roughness will be examined in greater detail not only from a viewpoint of vehicle occupant comfort but also from a viewpoint of the prolongation of the service life of pavement.

REFERENCES

Cebon, D., 1999. Handbook of Vehicle-Road Interaction, Swets & zeitlinger, Netherlands.

Heukelom,W. and Klomp,J,G., 1964. *Road Design and Dynamic Loading*, Proceedings of AAPT, Vol.33.

Ikeda, T. and Ito, M., 1985. *Estimating equations for tire pressure of truck.* Proceedings of the 40th Annual Meeting of Japan Society of Civil Engineers (JSCE) (in Japanese).

Japan Road Association, 2006. Pavement Design Handbook (in Japanese).

JSCE, 2005. Introduction to Pavement Structural Analysis Based on Multi-layered Elastic Systems (in Japanese).

Van der Poel, C., 1954. *A General System Describing the Visco-elastic Properties of Bitumen and its Relation to Routine Test Data*, Journal of Applied Chemistry, Vol.4.

Yonezawa, F., 1986. *Brownian Movement*, Kyoritsu publishing company (in Japanese)